Electronic Supplementary Information

Tuning Reactivity of Copper Complexes Supported by Tridentate Ligands Leading to Two-Electron Reduction of Dioxygen

Pattira Suktanarak,[a] Sarayut Watchasit,[b] Kantima Chitchak,[c] Nukorn Plainpan,[a] Kittipong Chainok,[d]
Parichatr Vanalabhpatana,[a,e] Prompong Pienpinijtham,[a] Chomchai Suksai,[f] Thawatchai Tuntulani,[a]
Vithaya Ruangpornvisuti,[a] and Pannee Leeladee[a,g,*]

[a] Department of Chemistry, Faculty of Science, Chulalongkorn University, Bangkok 10330, Thailand.

[b] Nuclear Magnetic Resonance Spectroscopic Laboratory, Science Innovation Facility, Faculty of Science, Burapha University, Chonburi 20131, Thailand.

[c] Program of Petrochemistry and Polymer Science, Faculty of Science, Chulalongkorn University, Bangkok 10330, Thailand.

[d] Materials and Textile Technology, Faculty of Science and Technology, Thammasat University, Pathum Thani 12121, Thailand.

[e] Electrochemistry and Optical Spectroscopy Center of Excellence, Department of Chemistry, Faculty of Science, Chulalongkorn University, Bangkok 10330, Thailand.

[f] Department of Chemistry and Center for Innovation in Chemistry, Faculty of Science, Burapha University, Chonburi 20131, Thailand.

[g] Research Group on Materials for Clean Energy Production STAR, Department of Chemistry, Faculty of Science, Chulalongkorn University, Bangkok 10330, Thailand.

Table **S1**. Crystal data and structure refinement for **2b**, **3a**, and **3b**.

	2b	**3a**	**3b**
Empirical formula	$C_{54}H_{46}C_{l4}Cu_2N_6O_8$	$C_{44}H_{42}Cl_4Cu_2N_8O_{16}$	$C_{44}H_{46}Cl_4Cu_2N_8O_{18}$
Formula weight	1175.85	1207.73	1243.77
Temperature/K	296.0	296.0	296.0
Crystal system	monoclinic	triclinic	triclinic
Space group	$P2_1/n$	$P-1$	$P-1$
a/Å	11.5432(11)	8.4013(6)	10.0380(3)
b/Å	12.0648(12)	9.4328(6)	10.6269(3)
c/Å	20.0110(18)	16.0385(11)	12.7725(4)
α/°	90	84.045(2)	109.7640(10)
β/°	94.684(3)	84.266(2)	95.8450(10)
γ/°	90	78.661(2)	97.6530(10)
V/Å^3	2777.6(5)	1235.36(15)	1254.94(7)
Z	2	1	1
ρ_{calc}g/cm^3	1.406	1.623	1.646
μ/mm^{-1}	1.015	1.156	1.143
F(000)	1204.0	616.0	636.0
Crystal size/mm^3	0.30 × 0.22 × 0.18	0.24 × 0.22 × 0.16	0.26 × 0.26 × 0.20
Radiation	MoKα (λ = 0.71073)	MoKα (λ = 0.71073)	MoKα (λ = 0.71073)
2θ range for data collection/°	6.186 to 52.872	5.768 to 50.846	2.9–27.8°
Reflections collected	51374	29505	42084
Independent reflections	5692	4537	5996
R_{int}, R_{sigma}	0.0934, 0.0460	0.1042, 0.0610	0.0401, 0.0260
Data/restraints/parameters	5692/202/371	4537/88/372	5996/195/419
Goodness-of-fit on F^2	1.023	1.031	1.024
Final R indexes [$I \geq 2\sigma(I)$]	$R_1 = 0.0448$, $wR_2 = 0.1120$	$R_1 = 0.0596$, $wR_2 = 0.1361$	$R_1 = 0.0430$, $wR_2 = 0.1074$
Final R indexes [all data]	$R_1 = 0.0693$, $wR_2 = 0.1240$	$R_1 = 0.1027$, $wR_2 = 0.1562$	$R_1 = 0.0618$, $wR_2 = 0.1175$
Largest diff. peak/hole / e Å^{-3}	0.47/−0.71	0.59/−0.59	0.60/−0.48

Table **S2**. Selected bond lengths and bond angles for **2b**, **3a**, and **3b**.

Complex 2b			
Cu1−N1	1.988(2)	Cu1−Cl1	2.2429(8)
Cu1−N2	2.031(2)	Cu1−Cl1^{i}	2.8396(9)
Cu1−N3	1.980(2)	Cu1−Cu1^{i}	3.5574(8)
Cl1−Cu1−Cl1^{i}	91.98 (3)	N2−Cu1−Cl1^{i}	91.65 (7)
N1−Cu1−Cl1^{i}	93.13 (7)	N3−Cu1−Cl1^{i}	87.85 (8)
N1−Cu1−Cl1	97.59 (8)	N3−Cu1−Cl1	96.97 (8)
N1−Cu1−N2	82.92 (10)	N3−Cu1−N1	165.37 (10)
N2−Cu1−Cl1	176.30 (7)	N3−Cu1−N2	82.45 (10)
Complex 3a			
Cu1−N1	1.963(4)	Cu1−N4	1.982(5)
Cu1−N2	2.032(4)	Cu1−O1	2.442(4)
Cu1−N3	1.978(4)	Cu1···Cu1^{ii}	7.7309(5)
N1−Cu1−N2	84.38(16)	N2−Cu1−N4	174.87(17)
N1−Cu1−N3	167.14(17)	N2−Cu1−O1	90.09(15)
N1−Cu1−N4	97.78(17)	N3−Cu1−N4	94.98(18)
N1−Cu1−O1	91.00(15)	N3−Cu1−O1	89.64(15)
N2−Cu1−N3	82.78(16)	N4−Cu1−O1	94.51(17)
Complex 3b			
Cu1−N1	1.981(2)	Cu1−N4	1.994(2)
Cu1−N2	2.035(2)	Cu1−O1	2.295(2)
Cu1−N3	1.993(2)	Cu1···Cu1^{ii}	8.9150(14)
N1−Cu1−N2	82.75(8)	N2−Cu1−N4	167.82(9)
N1−Cu1−N3	165.50(9)	N2−Cu1−O1	94.18(8)
N1−Cu1−N4	96.78(9)	N3−Cu1−N4	97.09(10)
N1−Cu1−O1	94.19(8)	N3−Cu1−O1	88.04(9)
N2−Cu1−N3	82.80(9)	N4−Cu1−O1	97.99(9)

Symmetry codes: (i) −*x*+1, −*y*, −*z*+1; (ii) −*x*, 1−*y*, 1−*z*.

Table S3. Hydrogen-bond geometry (Å, °) for **2b**, **3a**, and **3b**.

D−H···*A*	*D*−H	H···*A*	*D*···*A*	*D*−H···*A*
Complex 2b				
C4−H4···*Cg*1$^{\mathrm{i}}$	0.97	2.7788(16)	3.475(4)	139
C7−H7*A*···O3*B*$^{\mathrm{ii}}$	0.97	2.55	3.252(7)	129
C13−H13*A*···O4*B*	0.97	2.54	3.154(8)	121
C25−H25···*Cg*2$^{\mathrm{i}}$	0.97	2.9078(16)	3.720(4)	141
Complex 3a				
C6−H6*A*···O8*B*$^{\mathrm{iii}}$	0.97	2.52	3.176(11)	125
C6−H6*B*···O7*A*$^{\mathrm{iii}}$	0.97	2.47	3.247(15)	137
C3−H3···O7*B*$^{\mathrm{iv}}$	0.93	2.66	3.255(12)	123
C3−H3···O7*A*$^{\mathrm{iv}}$	0.93	2.41	3.112(15)	132
C1−H1···O6*B*	0.93	2.28	3.113(11)	149
C1−H1···O6*A*	0.93	2.31	2.986(12)	129
Complex 3b				
O1−H1*A*···O2*A*	0.92	2.12	2.998(5)	158
O1−H1*A*···O2*B*	0.92	2.02	2.922(11)	168
O1−H1*B*···O6*A*	0.92	1.89	2.806(4)	172
O1−H1*B*···O6*B*	0.92	2.14	2.992(16)	153
C2−H2···O2*B*$^{\mathrm{v}}$	0.93	2.40	3.031(9)	125
C7−H7*A*···O8*B*$^{\mathrm{vi}}$	0.97	2.41	3.15(2)	133
C12−H12···O9*A*$^{\mathrm{vii}}$	0.93	2.51	3.239(5)	136
C22−H22*A*···O5*A*$^{\mathrm{v}}$	0.96	2.43	3.125(6)	129
C22−H22*A*···O5*B*$^{\mathrm{v}}$	0.96	2.34	3.089(10)	135

Symmetry codes: (i) −*x*+3/2, *y*−1/2, −*z*+1/2; (ii) *x*+1, *y*−1, *z*; (iii) *x*+1, *y*−1, *z*; (iv) −*x*+1, −*y*+2, −*z*+1; (v) −*x*+1, −*y*+1, −*z*+1; (vi) −*x*+1, −*y*+2, −*z*+2; (vii) −*x*+1, −*y*+1, −*z*+2.

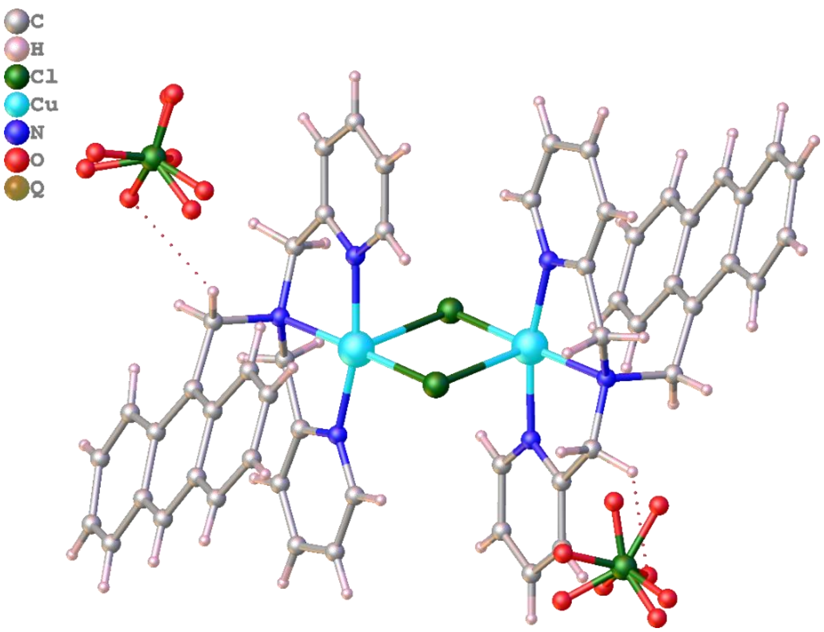

Fig. S1. Structure of compound $[Cu_2(\mu\text{-}Cl)_2(\mathbf{adpa})_2](ClO_4)_2$ (**2b**).

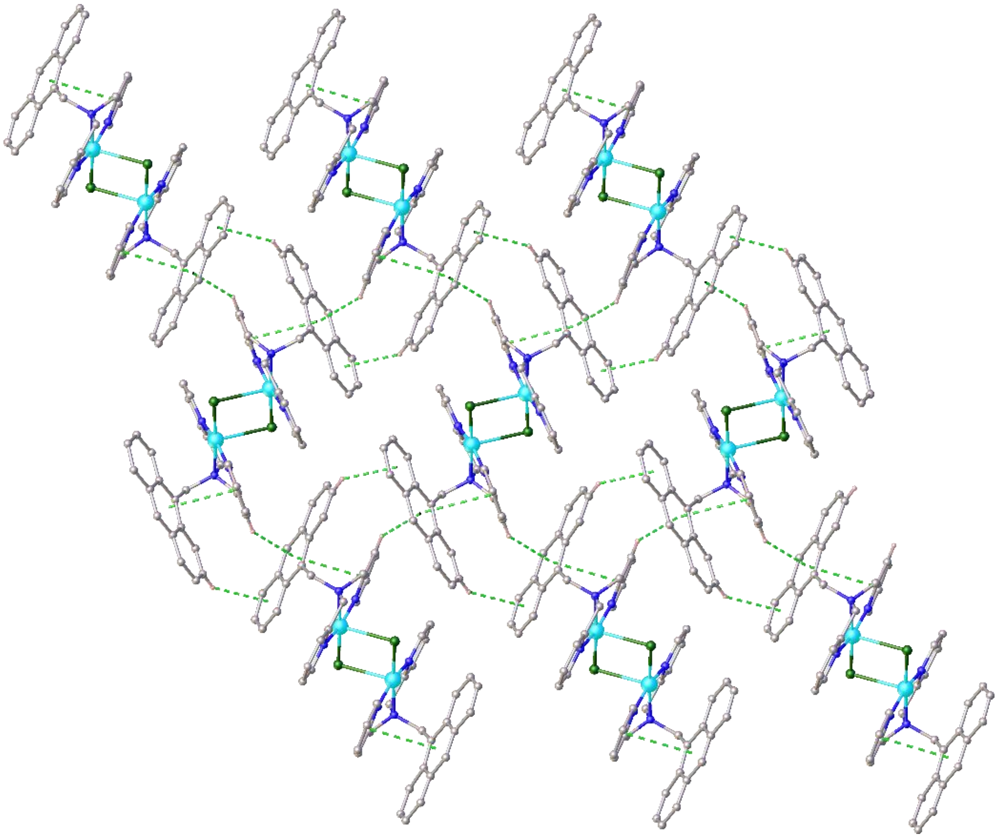

Fig. S2. View of the 2D sheets in **2b** generated by intramolecular π−π stacking and intermolecular C−H···π interactions

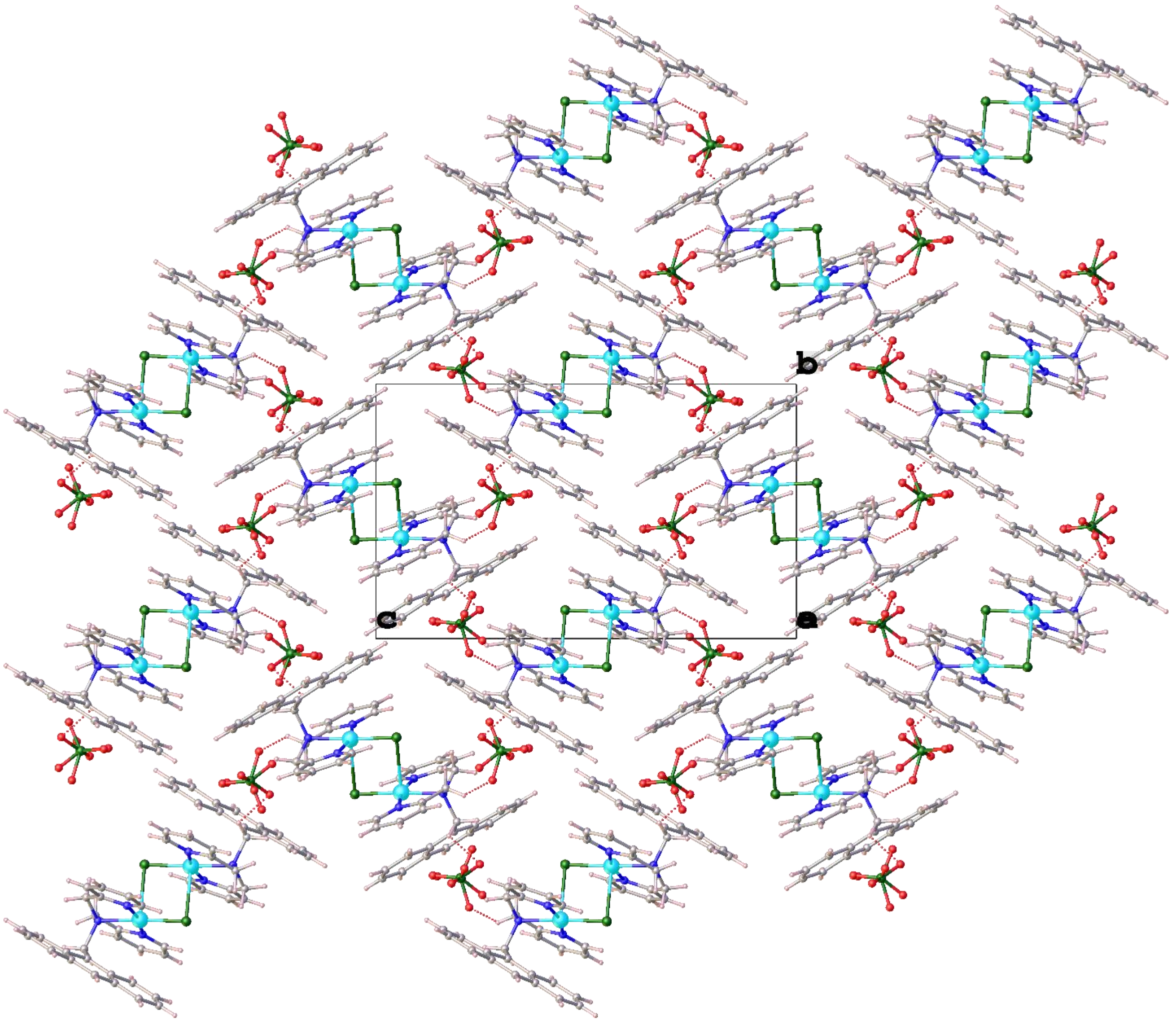

Fig. S3. Packing diagram in **2b** along the *a* axis, showing C−H···O hydrogen bonds.

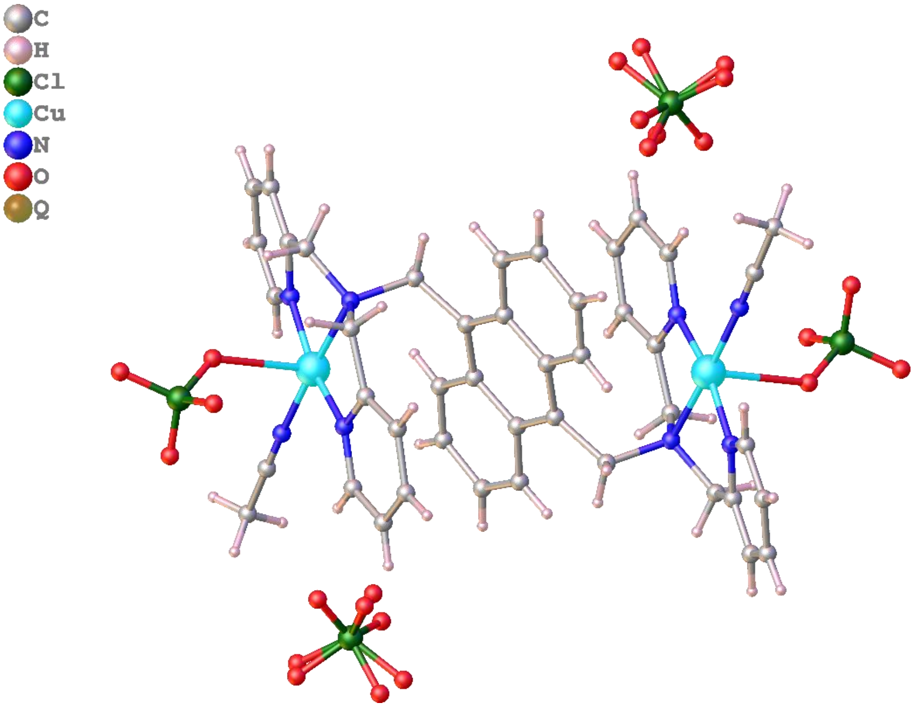

(a)

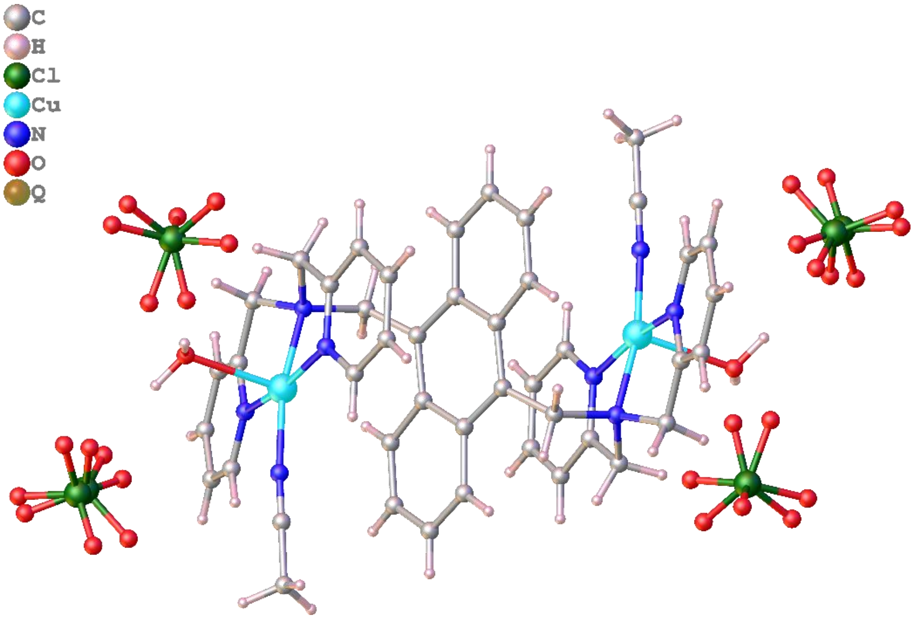

(b)

Fig. S4. Structure of compounds **3a** (a) and **3b** (b).

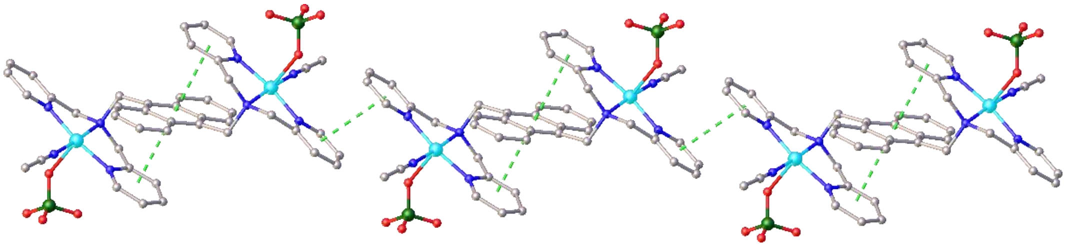

Fig. S5. View of the 1D chain in **3a**, generated π−π stacking interactions.

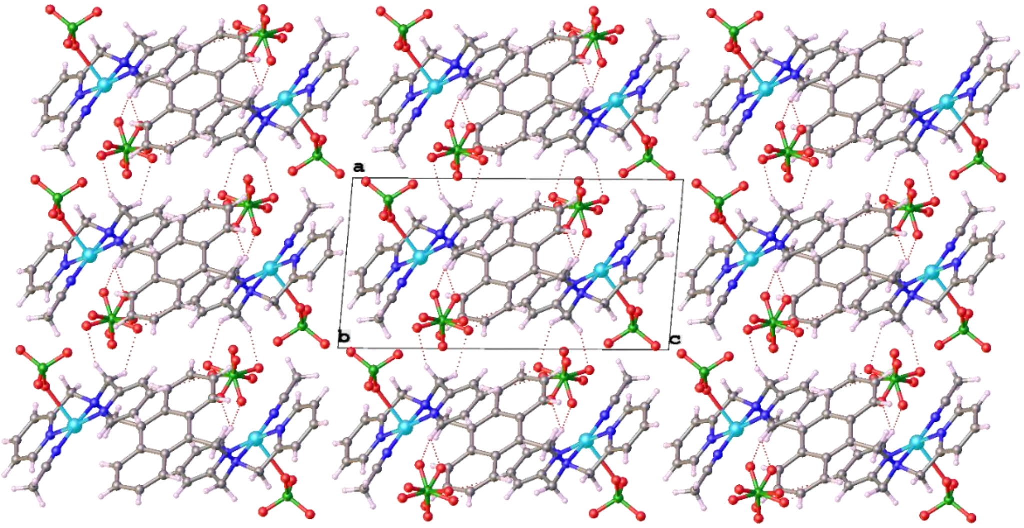

Fig. S6. Packing diagram in **3a** along the *b* axis, showing C−H···O hydrogen bonds.

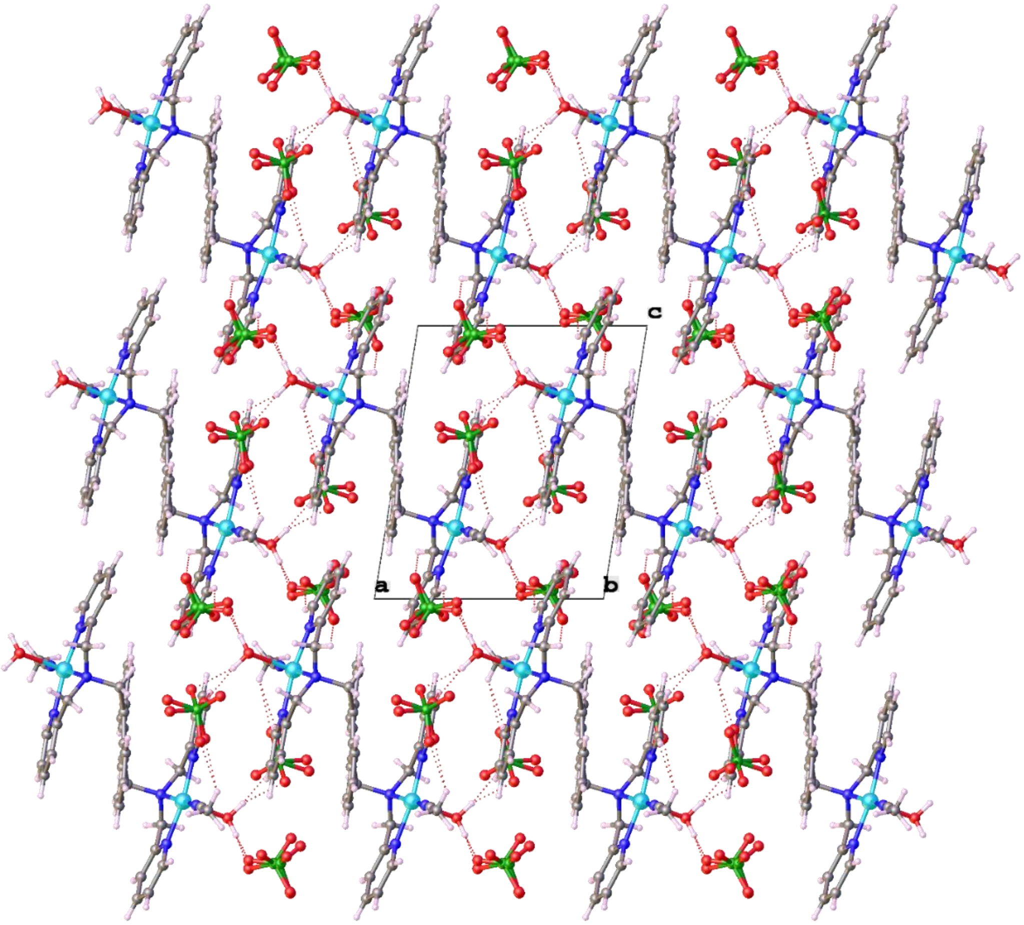

Fig. S7. Packing diagram in **3b** along the *b* axis, showing O−H···O and C−H···O hydrogen bonds.

Table S4. Areas under cyclic voltammetric curves for DMF–0.10 M TBAPF$_6$ solutions containing 1.00 mM **1**, **2a**, and **3a** recorded with a glassy carbon electrode (area = 0.071 cm^2) at 100 mV·s^{-1} from +0.30 to –1.20 to +0.30 V (Fig. 2)

Complex	Area (μA·V)	Charge (μC)
1	4.74	47.4
2a	4.86	48.6
3a	8.17	81.7

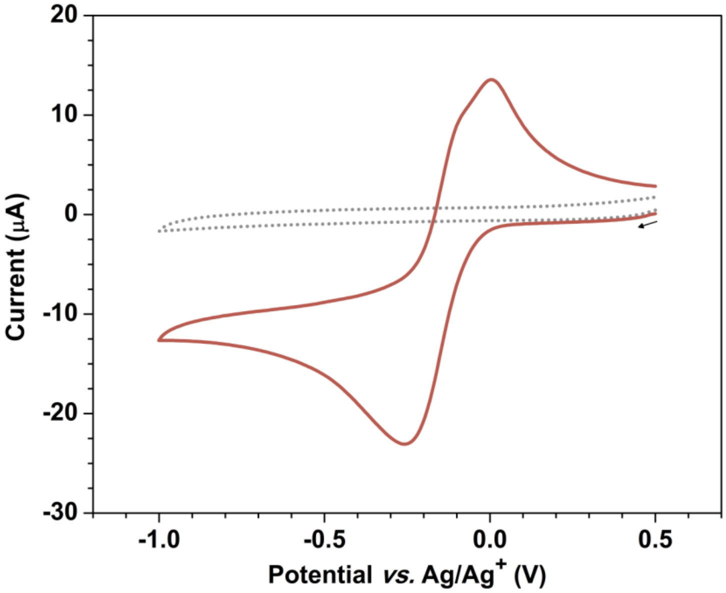

Fig. S8. Cyclic voltammograms recorded with a glassy carbon electrode (area = 0.071 cm^2) at 100 mV·s^{-1} from +0.50 to –1.00 to +0.50 V for CH$_3$CN solution containing 0.10 M TBAPF$_6$ (dotted line) and CH$_3$CN containing 0.10 M TBAPF$_6$ and 1.00 mM **3a** (solid line).

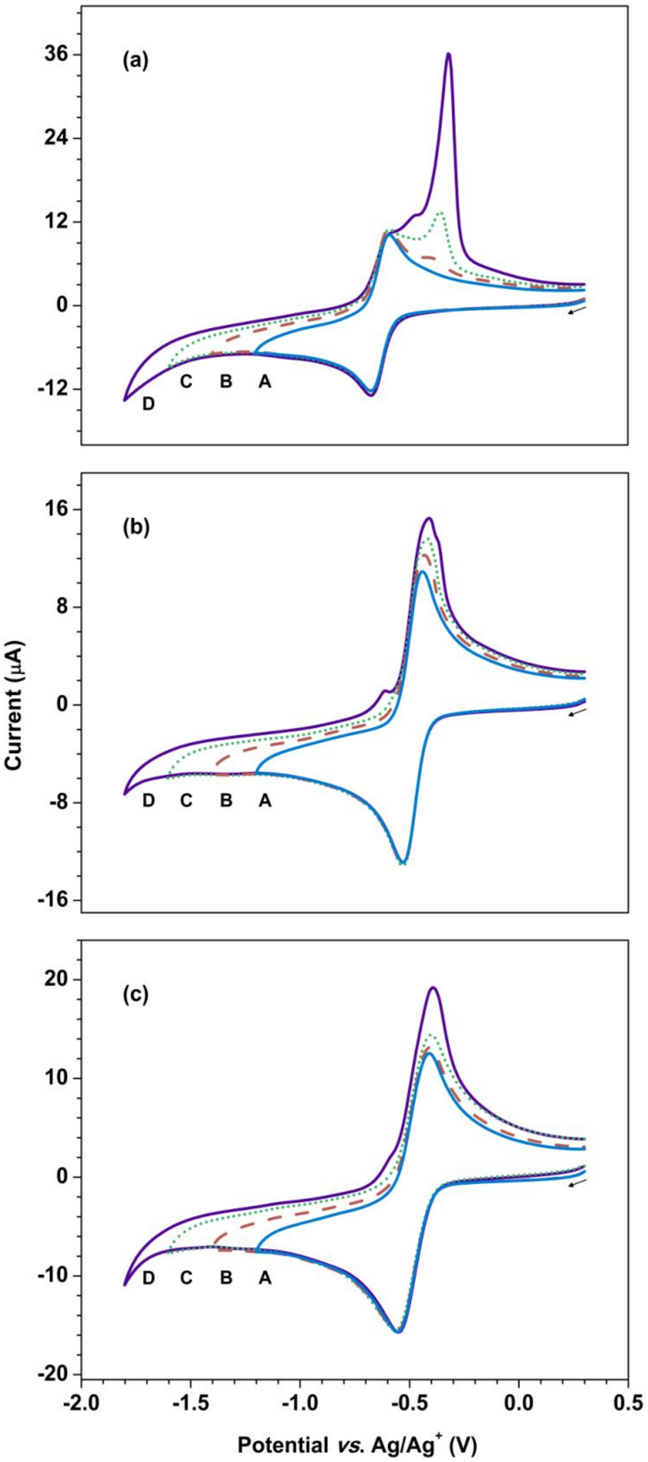

Fig. S9. Cyclic voltammograms for DMF containing 0.10 M $TBAPF_6$ in the presence of 1.00 mM (a) **1**, (b) **2a**, and (c) **3a** recorded with a glassy carbon electrode (area = 0.071 cm^2) at 100 $mV \cdot s^{-1}$ from (A) +0.30 to –1.20 to +0.30 V, (B) +0.30 to –1.40 to +0.30 V, (C) +0.30 to –1.60 to +0.30 V, and (D) +0.30 to –1.80 to +0.30 V.

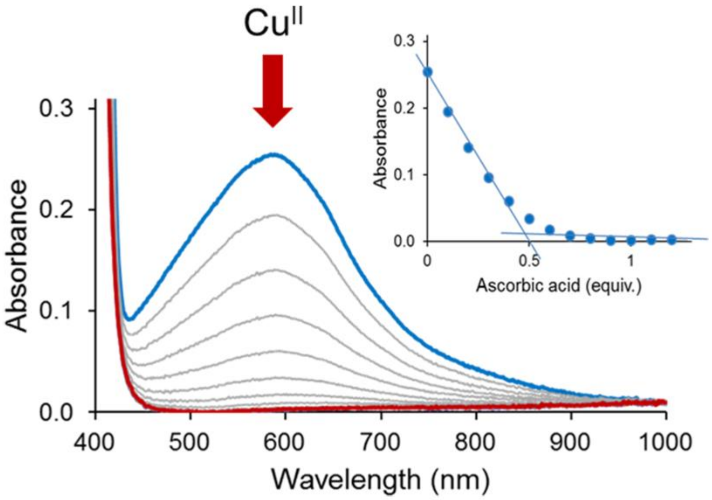

Fig. S10. UV-vis spectral changes upon addition of ascorbic acid (0 – 1.2 equiv) to **2a** solution (2 mM) in DMF/CH_3CN. The inset shows plot of Absorbance at 588 nm *vs*. equiv. of AsH_2 added.

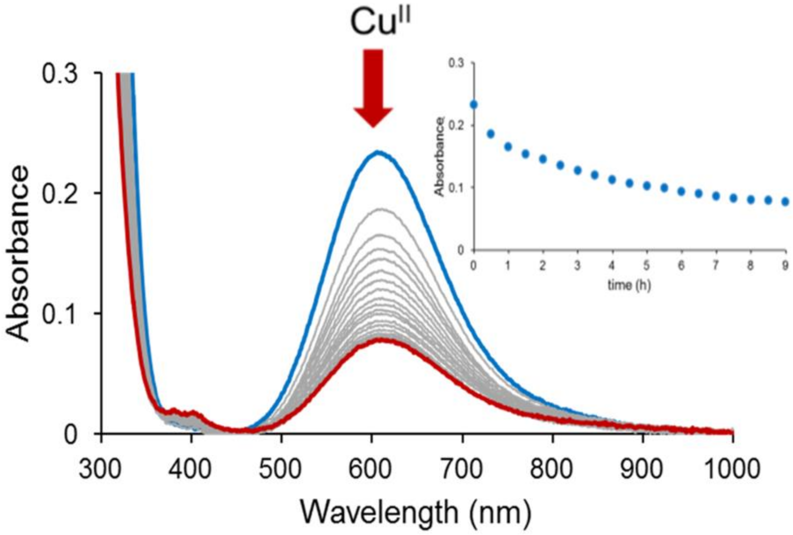

Fig. S11. UV-vis spectral changes upon addition of ascorbic acid (0.5 equiv) to compound **1** solution (2 mM) in DMF/CH_3CN. The inset shows plot of absorbance at 606 nm *vs*. times.

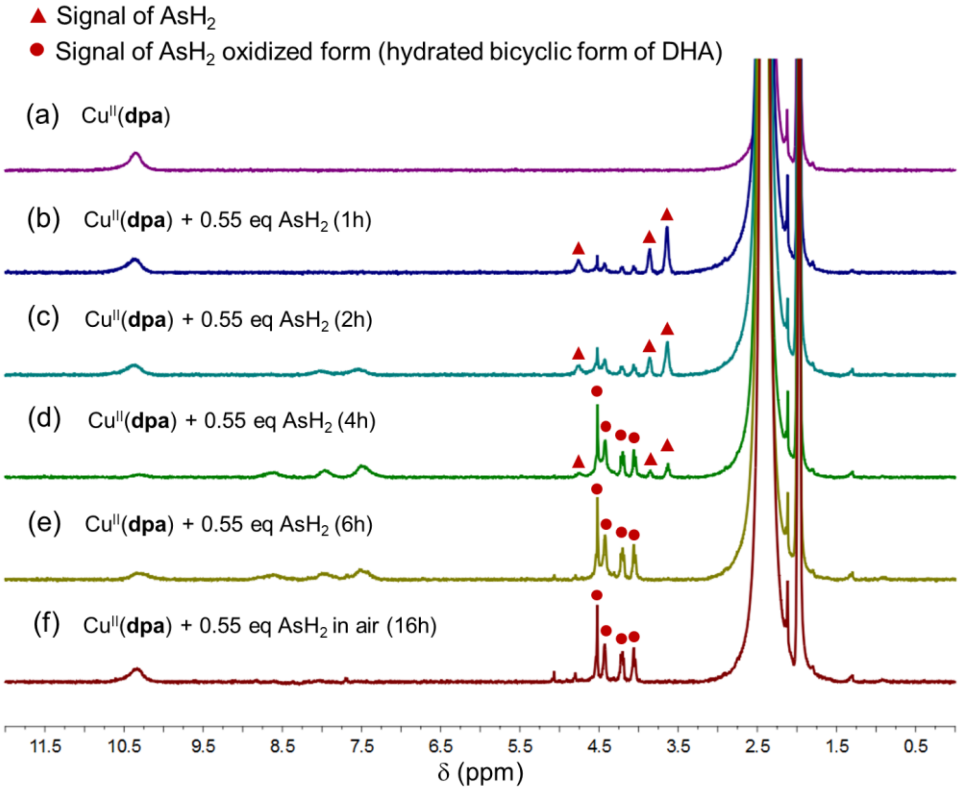

Fig. S12. ^{1}H-NMR spectra of compound **1** (a); a in the presence of ascorbic acid (0.55 equiv) in D_2O/CD_3CN (1-6 h) (b)-(e) and a after addition of ascorbic acid (0.55 equiv) in D_2O/CD_3CN under air for 16 h (f).

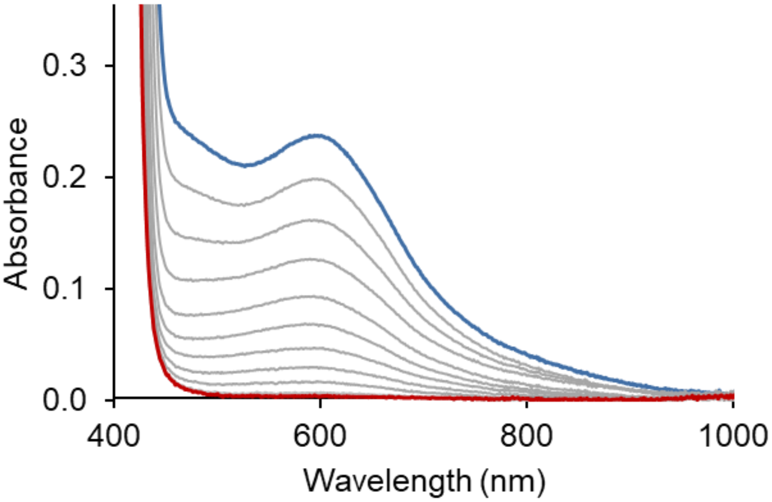

Fig. S13. UV-vis spectral changes of **3a** (1 mM) in CH_3CN in the presence of ascorbic acid (0 – 2 equiv) in H_2O/CH_3CN.

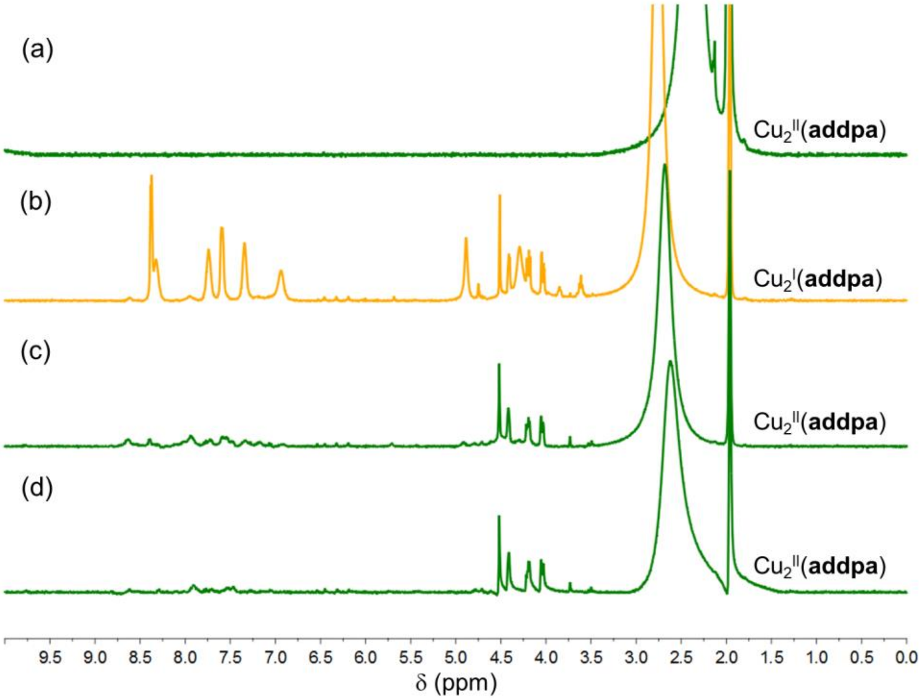

Fig. S14. ^{1}H-NMR spectra of (a) 10 mM **3a**; (b) upon the addition of ascorbic acid (1.5 equiv) to **3a** in d^7-DMF/CD_3CN; b exposed to O_2 for 1 h (c) and 2h (d).

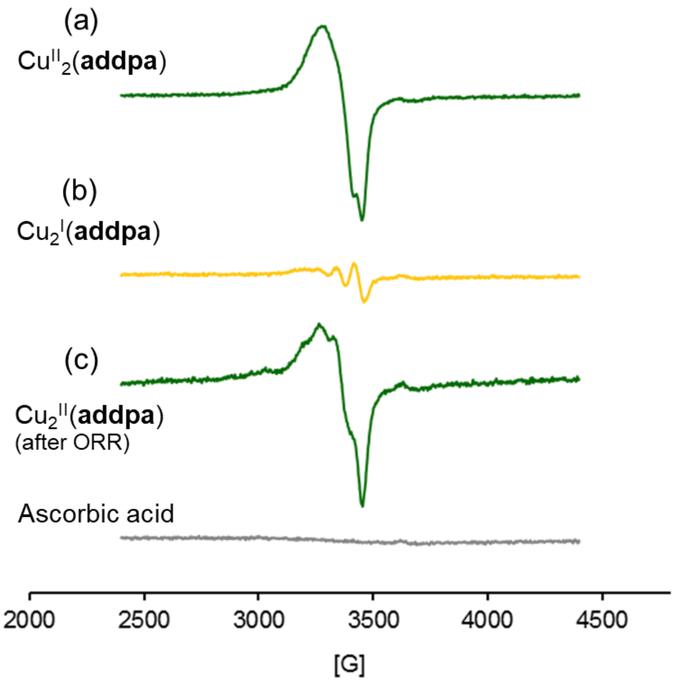

Fig. S15. EPR spectra of (a) 10 mM of **3a**, (b) **3a** in the presence of ascorbic acid (1.5 equiv.) in 15% DMF/CH_3CN and (c) **3a** after addition of ascorbic acid (1.5 equiv.) in CH_3CN under O_2. The EPR parameter: frequency= 9.838 GHz, microwave power= 0.620 mW, modulation amplitude= 5.00 G, modulation frequency= 100 kHz.

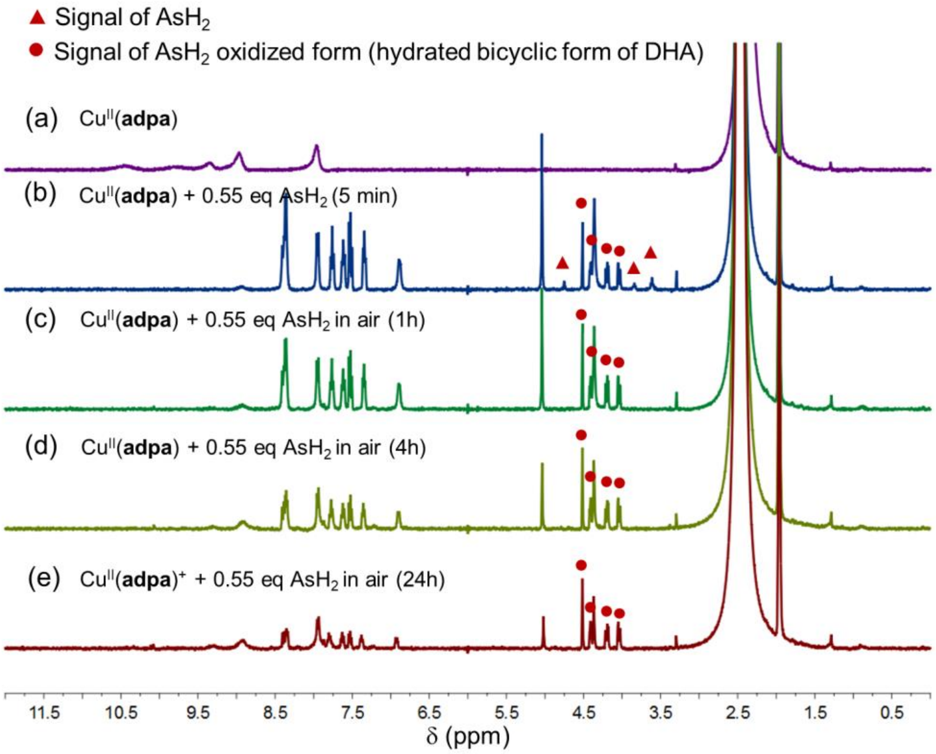

Fig. S16. ^{1}H-NMR spectra of (a) 10 mM **2a**; (b) upon the addition of ascorbic acid (0.55 equiv) to **2a** in D_2O/CD_3CN (5 min) and (c)-(e) b exposed to air for 1, 4 and 24 h.

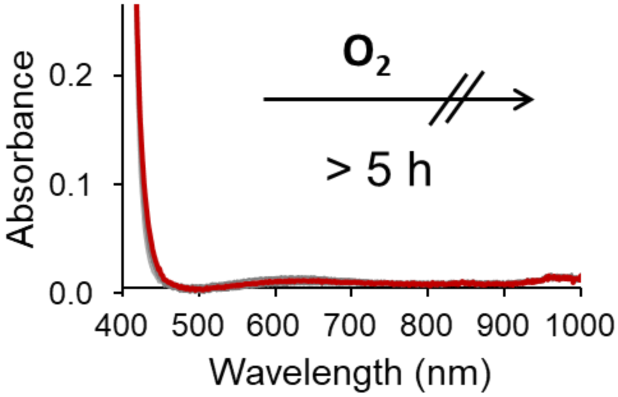

Fig. S17. UV-vis spectra of reaction between Cu^{I}(**adpa**) (2.0 mM) and ascorbic acid (0.55 equiv) in H_2O/CH_3CN after purging O_2 (0–5 h).

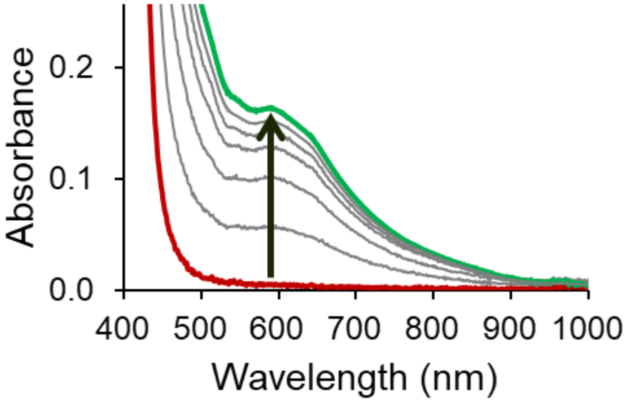

Fig. S18. UV-vis spectral change of reaction between Cu$^{I}_2$(**addpa**) (1.0 mM) and ascorbic acid (1.10 equiv) in H_2O/CH_3CN after purging O_2 (0–1 h).

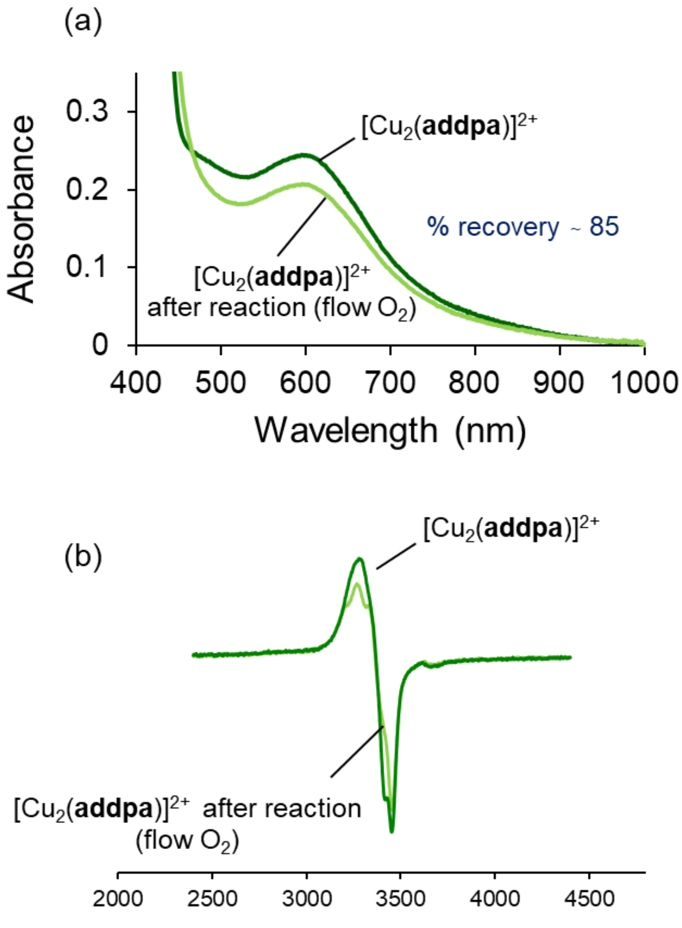

Fig. S19. (a) UV-vis spectra and (b) EPR spectra of **3a** before and after O_2 reduction.

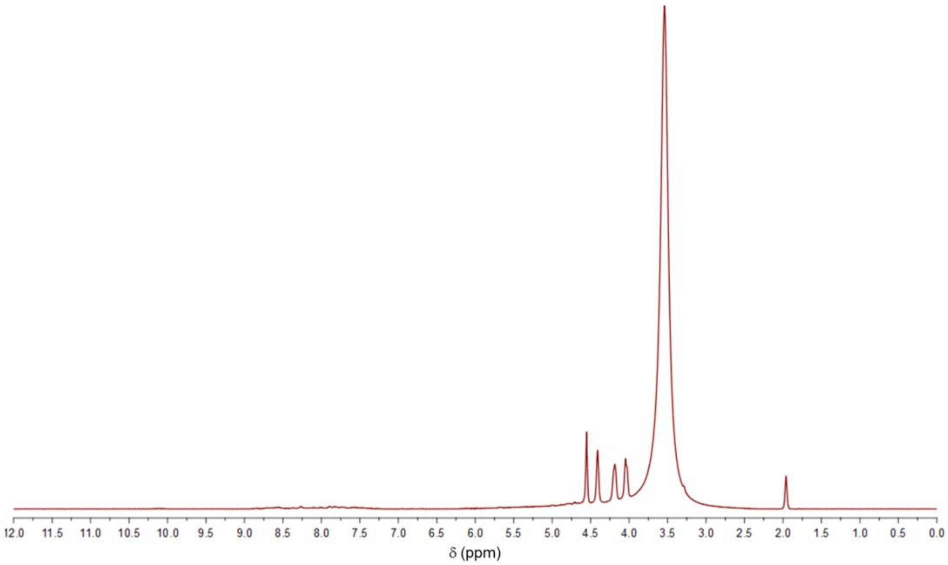

Fig. S20. ^{1}H-NMR of ORR catalyzed by **3a** upon the addition of 10 equiv. AsH_2 in 5% D_2O/CH_3CN. The reaction was prepared under O_2 gas for 90 min.

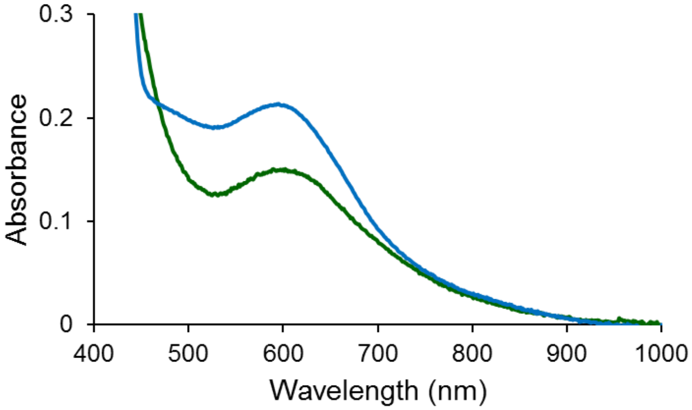

Fig. S21. UV-vis spectra of **3a** in CH_3CN (1mM) (blue line) and 1mM solution diluted from ORR reaction in the presence of excess O_2 and AsH_2 (10 equiv.) (green line).

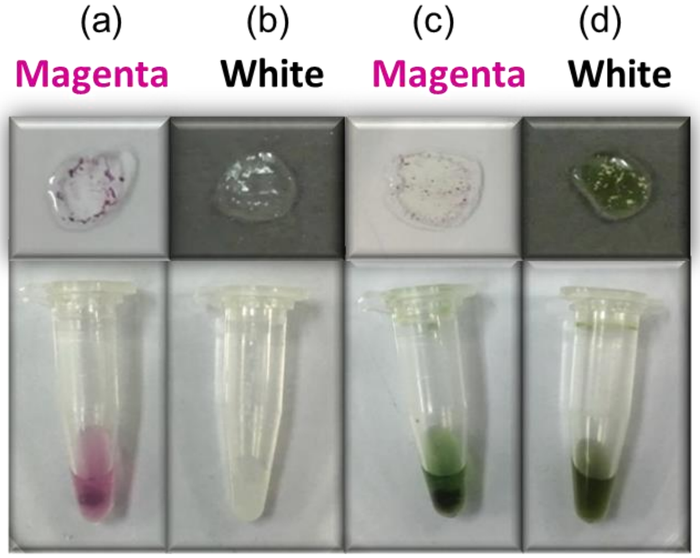

Fig. S22. Color change of (a) AgNPrs in CH_3CN; (b) AgNPrs in the presence of H_2O_2 (0.1 M); (c) AgNPrs in the presence of **3a** and (d) AgNPrs added to catalytic in ORR reaction (**3a** + 10 equiv. AsH_2 + excess O_2)

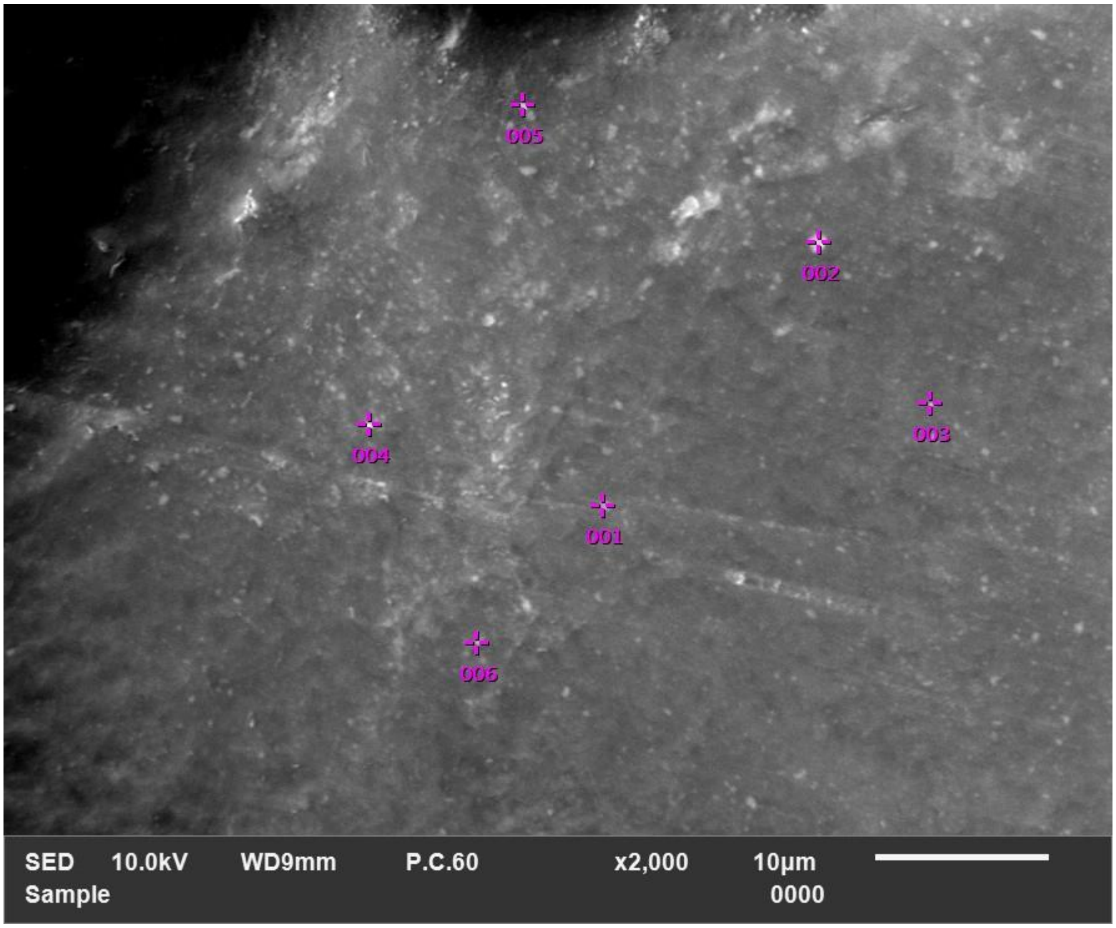

Fig. S23. Scanning electron microscopy (SEM) micrograph of magenta precipitates (AgNPrs)

Table S5. Element composition of AgNPrs analyzed by EDX technique

Point	**001**	**002**	**003**	**004**	**005**	**006**
% mass (C)	77.65	75.74	75.74	68.48	76.01	73.73
% mass (O)	16.54	16.05	16.05	14.92	17.27	15.55
% mass (Ag)	4.47	1.15	1.15	1.72	1.30	1.50
% mass (Na)	0.87	7.06	7.06	14.89	5.42	8.74

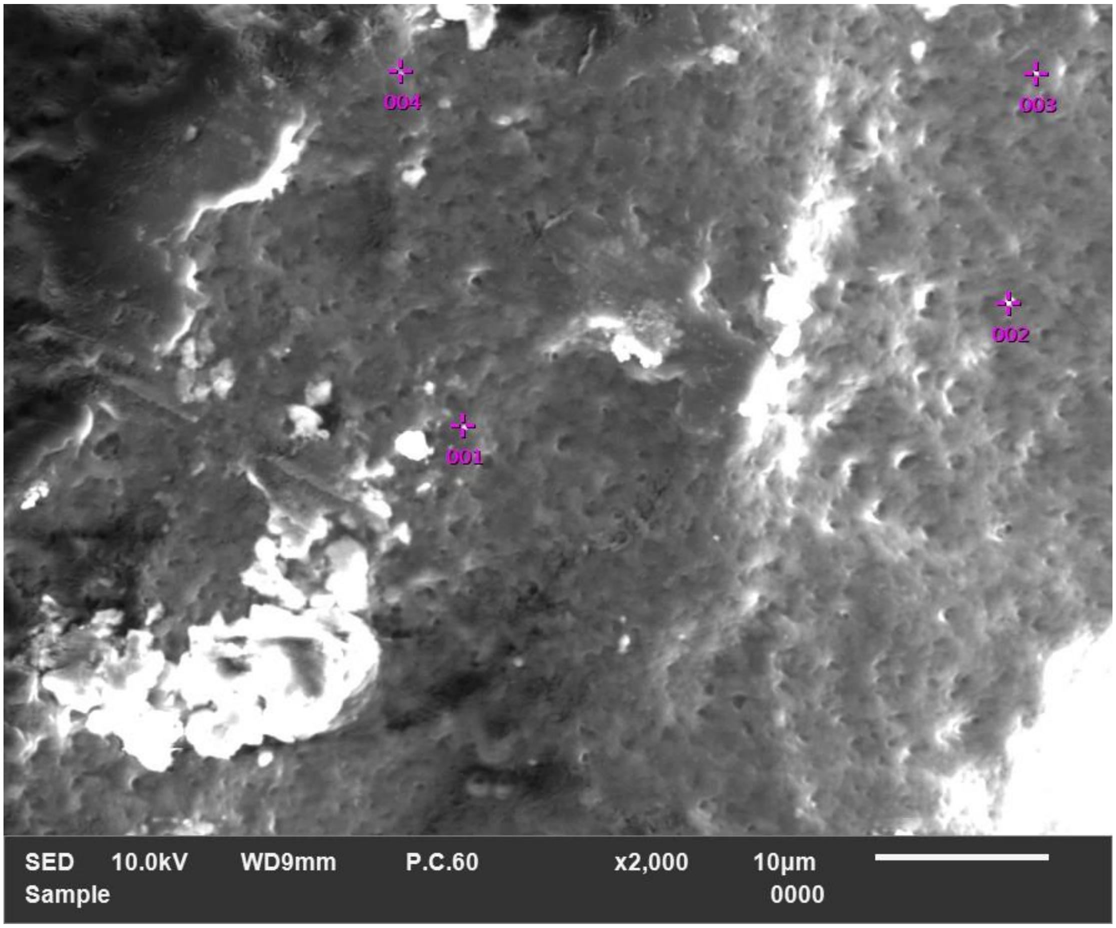

Fig. S24. Scanning electron microscopy (SEM) micrograph of white precipitates (AgNPrs + H_2O_2)

Table S6. Element composition of white precipitates analyzed by EDX technique

Point	**001**	**002**	**003**	**004**
% mass (C)	73.96	32.10	65.17	74.81
% mass (O)	22.43	11.26	21.65	23.65
% mass (Ag)	3.61	54.41	12.06	1.02
% mass (Na)	-	0.41	0.88	0.52

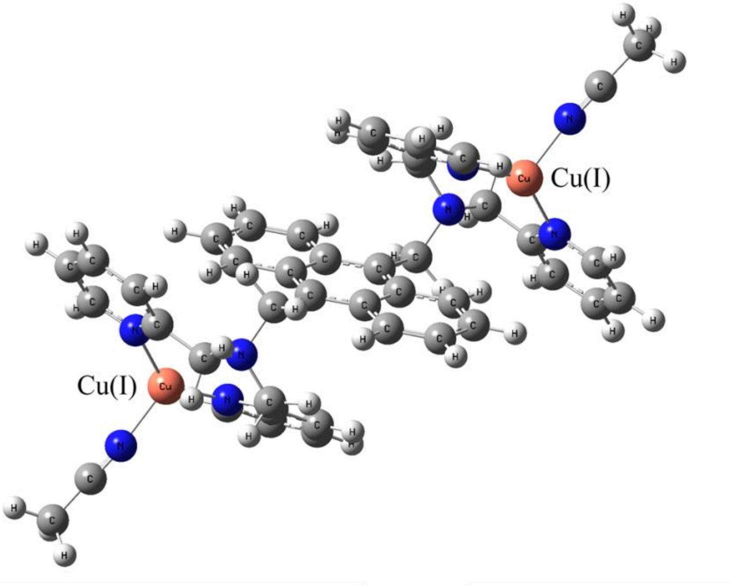

Fig. S25. The CPCM(UFF)/B3LYP/6–31G(d,p)–optimized structures in CH$_3$CN of Cu$^{I}_{2}$(**addpa**)

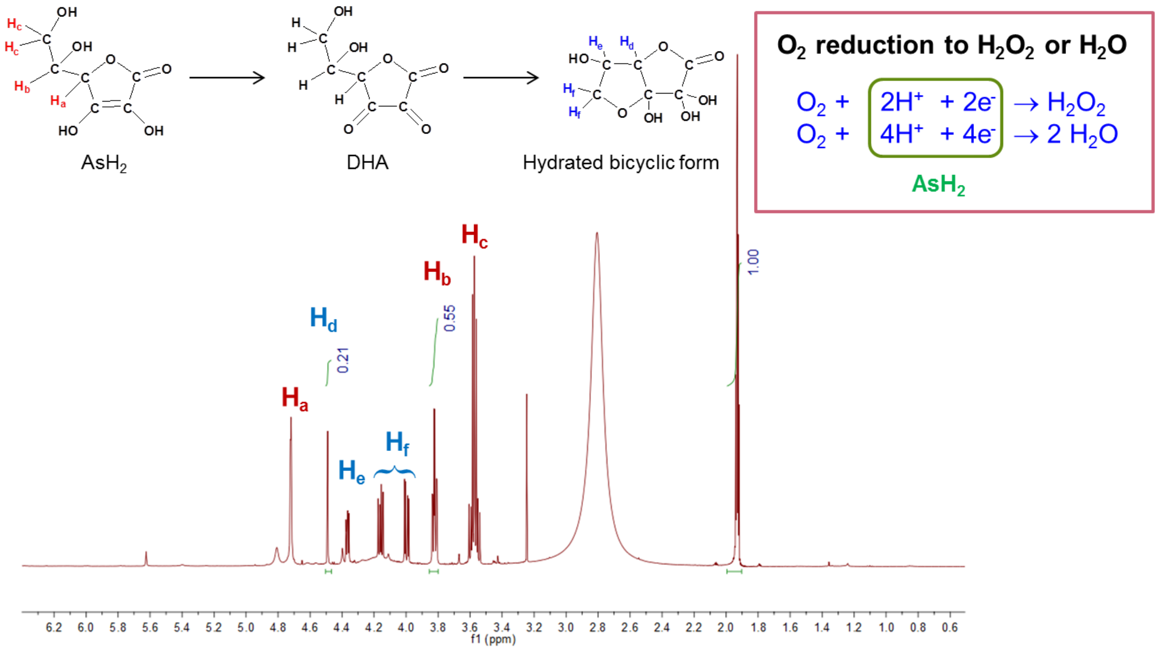

Fig S26. ^{1}H-NMR spectrum for determination of electron transferred in ORR catalysed by Cu_2(**addpa**) (6mM) in O_2-saturated solvent (5% D_2O/CD_3CN)

Table **S7** Calculation for number of electrons consumed in oxygen reduction

$[O_2]$ (mM)*	Number of e^- used per O_2 molecule
12.1 ± 0.7[1]	1.9 e^-
9.6 ± 0.5[2]	2.4 e^-

*The concentration of O_2 saturated in CH_3CN was obtained from the literature.

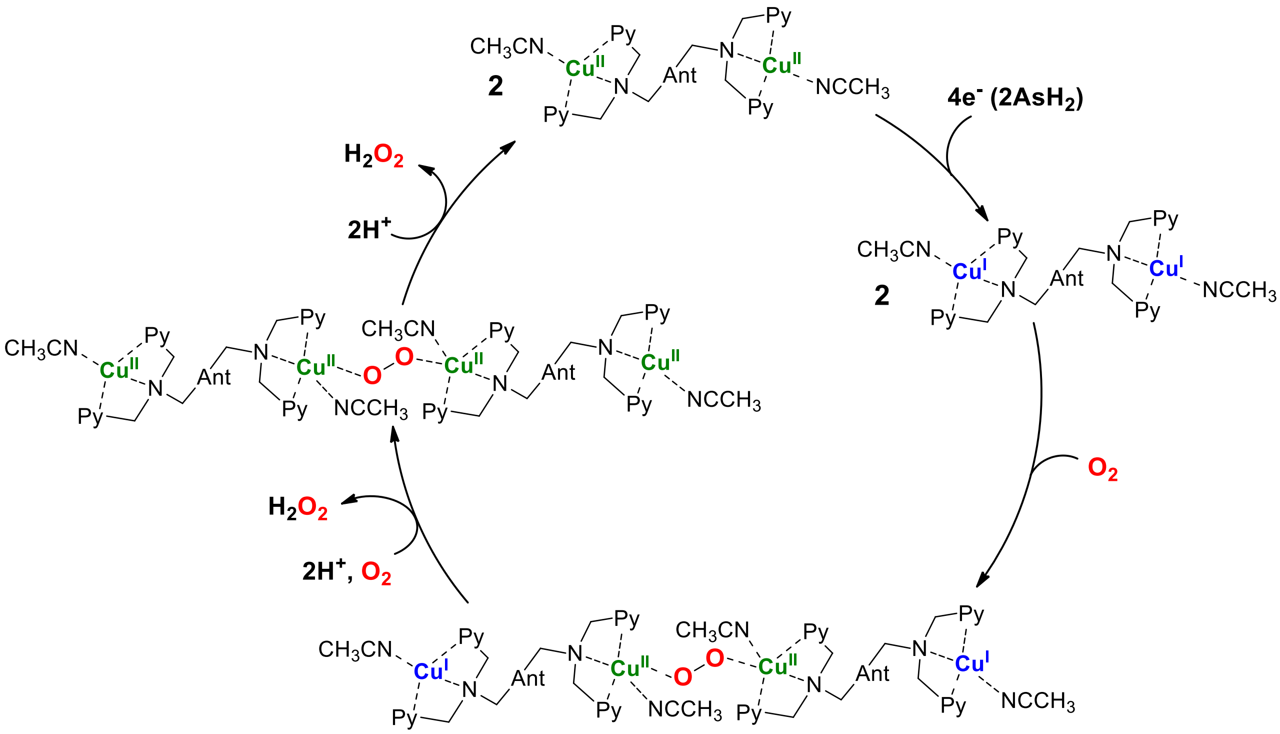

Fig. S27. Proposed mechanism for ORR mediated by Cu_2(**addpa**)

References:

1. S. Horstmann, A. Grybat and R. Kato, *J. Chem. Thermodyn.*, 2004, **36**, 1015-1018.
2. C. Franco and J. Olmsted, *Talanta*, 1990, **37**, 905-909.